Journal of Materials Chemistry A

ROYAL SOCIETY OF CHEMISTRY

PAPER

View Article Online
View Journal | View Issue

Cite this: J. Mater. Chem. A, 2023, 11, 789

Determination of layered nickel hydroxide phases in materials disordered by stacking faults and interstratification†

Kurt Lawson, [a] Samuel P. Wallbridge, [a] Amy E. Catling, [a] Caroline A. Kirk[b] and Sandra E. Dann*[a]

The formation of stacking faults and phase interstratification disorder in layered nickel(II) hydroxides during the chemical precipitation synthesis of materials using nickel(II) nitrate and potassium hydroxide solutions has been investigated in the temperature range of 5 °C to 95 °C and time intervals from 1 hour to 1 week. Stacking faulted materials were identified by broadening of the 00*l* reflections, while interstratified materials were identified through the splitting of the 001 into two lines. In contrast to the disorder concepts presented in previous studies of these materials, this work has shown through vibrational spectroscopy that both the alpha-phase and beta-phase hydroxides are present in materials described with stacking fault disorder, while layered hydroxysalts were additionally present in the materials considered to be interstratified. Standard mixtures of $Ni_3(OH)_4(NO_3)_2$ and β-$Ni(OH)_2$ were prepared to investigate if the intensity of particular vibrational bands could be correlated with the proportion of the particular phases in mixtures. The intensities of the C_{2v} nitrate infrared and Raman bands at 990 cm^{-1} and 1315 cm^{-1} were shown to correlate with the amount of layered hydroxynitrate incorporated in the phase, theoretically providing a method to determine the components in mixed compositions. Since disorder and phase impurities in layered nickel hydroxide materials affect both their electroactive stability and performance as cathode materials, this work has important implications in several research fields.

Received 29th September 2022
Accepted 5th December 2022

DOI: 10.1039/d2ta07655a

rsc.li/materials-a

Introduction

Electroactive layered nickel hydroxides have applications as the cathode material of rechargeable batteries,[1] supercapacitors,[2–5] electrochromic devices,[6] and electrocatalysts.[7] Two structures are commonly described for nickel hydroxide, a well-defined crystalline beta-phase and a poorly crystalline alpha-phase; the structure of the latter is not fully understood.[8,9] The beta-phase of nickel hydroxide, β-$Ni(OH)_2$, exists naturally as the emerald green coloured mineral theophrastite[10] and is isostructural with $Mg(OH)_2$ (brucite) and $Ca(OH)_2$ (portlandite), and crystallises with the cadmium iodide (CdI_2) type structure.[11–13] The layered structure consists of a hexagonal close-packed (hcp) arrangement of the oxide anions with the nickel(II) cations on the octahedrally coordinated sites and the hydrogen of the hydroxide on the tetrahedral sites directed towards the adjacent layer.[11,14] Alpha-phase nickel hydroxide, α-$Ni(OH)_2$, is also a layered structure with the same edge-sharing octahedral layers as β-$Ni(OH)_2$.[15] Due to the relatively weak interactions between the layers, species can be intercalated between the layers resulting in an elongation along the *c*-direction of the unit cell. This also causes the layers to slip out of alignment and randomly orient relative to one another which can result in a structure often described as turbostratic.[16,17] The crystal structures of β-$Ni(OH)_2$ and α-$Ni(OH)_2$ are shown in Fig. 1 (ref. 18 and 19) with ideal layer stacking given to α-$Ni(OH)_2$ to highlight the different distances between adjacent octahedral layers that allow for water and anionic species to intercalate.

In addition, there are also disordered structures reported for layered nickel hydroxides including those with stacking faults and phase interstratification disorder as shown in the diagrams in Fig. 2. Stacking faults typically result in disorder of the crystallographic planes in the material. This phenomenon is encountered in layered metal hydroxides due to strong intra-layer bonding and relatively weak interactions between them, typically causing misalignment of the layers in the *c*-direction. Beta-phase nickel hydroxides with stacking fault disorder are sometimes simply described as being 'badly crystalline' in the literature.[9,17] Interstratified structures have been said to occur when the beta-phase and alpha-phase layer hydroxide materials are stacked in the *c*-direction of the unit cell within a single crystallite.

[a]Department of Chemistry, Loughborough University, Loughborough, UK. E-mail: S.E.Dann@lboro.ac.uk

[b]School of Chemistry, University of Edinburgh, Edinburgh, UK

† Electronic supplementary information (ESI) available. See DOI: https://doi.org/10.1039/d2ta07655a

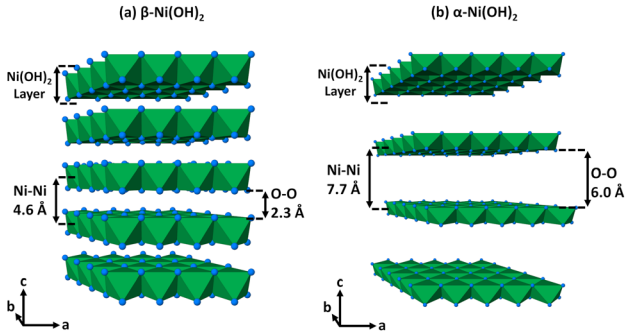

Fig. 1 Crystal structures drawn of (a) β-$Ni(OH)_2$ and (b) α-$Ni(OH)_2$ with ideal layer stacking to highlight the difference between the interlayer spacing adapted after data of the minerals theophrastite and jamborite respectively.[18,19] Nickel(II) cations form coordination octahedra (green) with the oxygen of the hydroxide groups (blue spheres). β-$Ni(OH)_2$ crystallises in the $P\bar{3}m1$ space group with dimensions of a, $b = 3.11$ Å and $c = 4.62$ Å with α, $\beta = 90°$ and $\gamma = 120°$ while ideal α-$Ni(OH)_2$ crystallises in the $R\bar{3}m$ space group with dimensions of a, $b = 3.07$ Å and $c = 23.2$ Å with α, $\beta = 90°$ and $\gamma = 120°$.

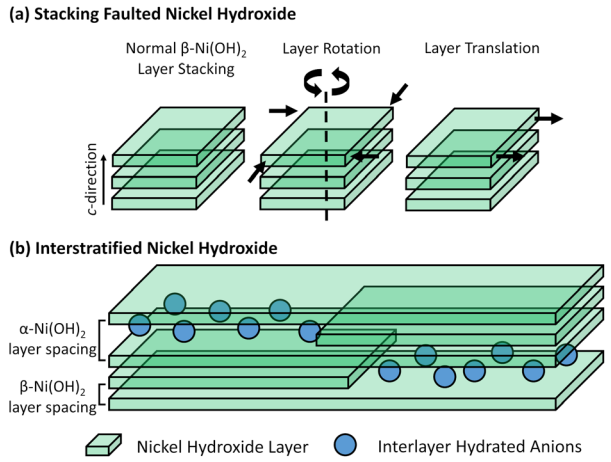

Fig. 2 (a) Diagram of stacking fault disorder in adjacent beta-phase nickel hydroxide layers (left) including rotation about the c-axis (centre) and translation in the ab-plane (right).[34] (b) Diagram of the phase interstratification that occurs within a single crystal of nickel hydroxide highlighting regions of beta-phase as well as alpha-phase nickel hydroxide with intercalating species.[40]

The study of disordered nickel(II) hydroxides is often challenging due to the poorly crystalline nature of these materials, thus limiting the utility of powder diffraction methods, and the determination of the phases present in a mixed-phase material can be difficult. The hypothetical structure and concomitant conducting properties of the alpha-phase hydroxide, with formula $Ni(OH)_{2-x}(H_2O)_x(A^{n-})_{x/n}$, results from the movement of mobile protons in the partially protonated hydroxide layer leading to very low levels of weakly coordinated anions (*ca.* $x = 0.1$) between the layers[20] to counteract the charge from the itinerant protons. Other phases of the form $M(OH)_{2-x}(A^{n-})_{x/n}$ that are derived from the parent brucite structure also exist, but with some of the hydroxides partially substituted for other anionic species that coordinate directly to the metal cations. Layered nickel hydroxynitrates are formed when the hydroxyl anions are substituted for nitrate and the three different compositions previously described are $Ni_2(OH)_3(NO_3)$ where $x = 0.5$,[21] $Ni_3(OH)_4(NO_3)_2$ where $x = 0.67$,[22] and $Ni(OH)(NO_3)$ where $x = 1.0$.[23] While the structures of the nickel-containing analogues have not yet been determined, diffraction and compositional evidence in the literature suggest that these phases are isostructural with analogous layered metal hydroxynitrates with the same x value. The structures of $Cu_2(OH)_3(NO_3)$ where $x = 0.5$,[24] $Zn_3(OH)_4(NO_3)_2$ where $x = 0.67$,[25] and $Zn(OH)(NO_3)\cdot H_2O$ where $x = 1.0$ (ref. 26) are shown in Fig. 3. Alpha-phase hydroxides differ from layered hydroxysalt structures because the anion incorporation and subsequent hydration are variable and often lower, with these anions not bound to the cations. While alpha-phases also share similarities with hydrotalcite-type layered double hydroxide structures, they also differ from them by containing no trivalent cations.[20]

Due to the growing interest in the use of nickel oxides and hydroxides for electrochemical applications, the purity of the hydroxide phases is important and can affect the performance of compounds prepared from them, *e.g.* $LiNiO_2$ for use in lithium-based batteries.[27] Therefore, methods to distinguish between different hydroxide phases and estimate the amount of an impurity phase are of interest. Since the nickel hydroxide that is formed by the chemical precipitation method is dependent on the conditions, herein we investigate the nickel hydroxide phases and disorder formed from hydrated nickel(II) nitrate and base as a function of synthesis temperature and time. Material analysis using powder X-ray diffraction methods shows features in the data that are typically expected of stacking fault and phase interstratification behaviour with local structure synchrotron techniques additionally offering no further information about the structures formed. Analysis performed using infrared and Raman spectroscopy provided new insight into the phases present in these materials and show that mixed-phase samples may be easily mistaken for disorder in the materials. This emphasises the need to employ extra materials characterisation methods in addition to diffraction techniques for layered hydroxides that can successfully identify the presence of these poorly crystalline phases in a material.

Experimental section

Nickel hydroxide preparations

Nickel hydroxide phases were prepared as powders (*ca.* 1 g) by the homogenous precipitation synthesis method[1] where aqueous potassium hydroxide (86%, Fischer Chemical) solutions (25 mL, 0.25 M or 0.50 M) were added slowly to aqueous nickel(II) nitrate (99%, Acros Organics) solutions (25 mL, 0.25 M). The desired synthesis temperatures were reached using a temperature-controlled refrigerator at 5 °C or an oven for temperatures at 50 °C and 95 °C. The precipitate that formed was collected by gravity filtration and was washed with water (*ca.* 250 mL) until the filtrate was neutral. The solid green product was dried at ambient temperature for 48 h.

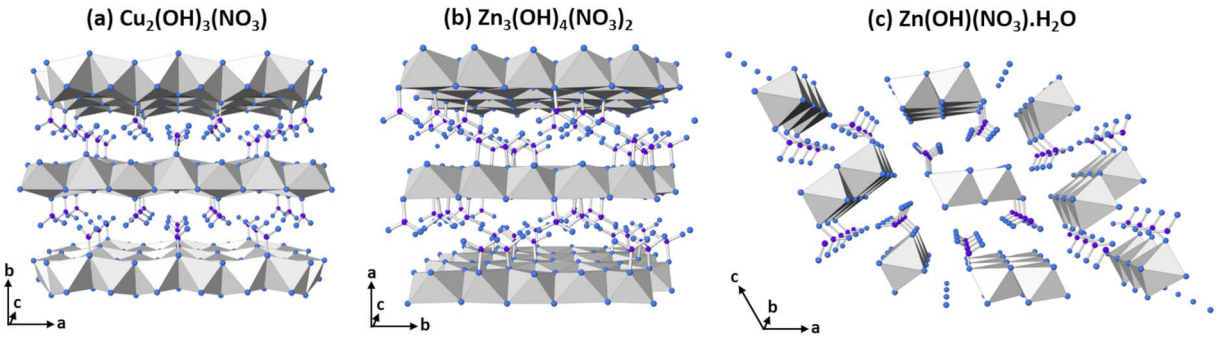

Fig. 3 The crystal structures of the layered hydroxynitrate phases (a) $Cu_2(OH)_3(NO_3)$ (gerhardtite) where $x = 0.5$, (b) $Zn_3(OH)_4(NO_3)_2$ where $x = 0.67$, and (c) $Zn(OH)(NO_3)\cdot H_2O$ where $x = 1.0$. Metal(II) cations form coordination octahedra (grey) with the oxygen (blue spheres) of the hydroxide groups or the nitrate groups (nitrogen are purple spheres).

The nickel hydroxynitrate phase $Ni_3(OH)_4(NO_3)_2$ was prepared as a powder (*ca.* 5 g) by the thermolysis method described by Biswick *et al.*[28] involving heating nickel(II) nitrate hexahydrate (*ca.* 5 g) in an oven at 220 °C for 2 h with stirring every 15 min. The solid product was cooled, washed with anhydrous ethanol (*ca.* 500 mL) then dried at 120 °C for 48 h.

Instrumentation

Powder X-ray diffraction (XRD) patterns were collected using a Bruker D8 Advance powder diffractometer with monochromatic Cu $K_{\alpha 1}$ radiation ($\lambda = 1.5406$ Å). The data were collected using a quartz standard calibrated Lynxeye detector over the 5–55° 2θ range with a step size of 0.014° 2θ. The International Centre for Diffraction Data (ICDD) powder diffraction file (PDF) database was used for phase identification.

Synchrotron X-ray pair distribution function (XPDF) data were collected on the I15-1 beamline at Diamond Light Source, Didcot, UK. The powder samples (*ca.* 1–10 mg) were loaded into quartz capillaries with a diameter of 1.5 mm (internal radii 0.65 mm). Diffraction data were collected using a wavelength of 0.161669 Å that was filtered to 10% flux (12.5% actual) using aluminium plates at ambient temperature over 300 s. The scattering data ($1.0 \leq Q \leq 30.0$ Å^{-1}) were processed into pair distribution function data using the GudrunX (2017) software.

Infrared (IR) absorption spectra were collected between 4000–250 cm^{-1} using a PerkinElmer Spectrum 100 FT-IR Spectrometer fitted with caesium iodide (CsI) optics. Potassium bromide (KBr) discs were initially used to record the spectra following previous literature methods but the KBr medium was abandoned and replaced with CsI. This was because KBr reacts with layered hydroxide phases,[21,29] resulting in nitrate bands at ~1380 cm^{-1} in all of the materials analysed regardless of the nitrate anion symmetry present.

Raman (R) data were collected between 4000–100 cm^{-1} using a Horiba Jobin Yvon HR LabRAM system in the backscatter configuration with a laser line at 633 nm originating from an argon ion (Ar^+) laser filtered to 10% power so as not to heat and decompose the sample. The laser was focused onto the sample to a spot size of 1 μm.

Thermogravimetric analysis (TGA) measurements were carried out using a TA instruments SDT Q600 with sample masses of between 10–20 mg and a reference of alumina (Al_2O_3). A temperature ramp method was used with a heating rate of 5 °C min^{-1} and a gas flow of 100 mL min^{-1}. Nickel hydroxide samples were heated under nitrogen to form nickel(II) oxide decomposition products.

Results and discussion

Identification of disordered nickel hydroxide materials

The nickel hydroxide synthesis temperature, chemical ageing duration and reagent concentrations were based on preliminary studies (Tables S1 and S2†). Initially, five temperature intervals (5 °C, 25 °C, 50 °C, 75 °C and 95 °C) and six chemical ageing durations (1 h, 6 h, 1 d, 2 d, 4 d, 1 w) were investigated. Powder X-ray diffraction analysis of these thirty materials indicated crystalline beta-phases were typically formed at both higher temperatures and longer ageing times, while poorly crystalline materials were formed at lower temperatures and shorter ageing durations. Several mixed phase materials were also

Table 1 Summary of the targeted nickel hydroxide materials prepared

	Material assigned	Description	Synthesis conditions	$Ni^{2+}:OH^-$ ratio
i	β-$Ni(OH)_2$	Beta-phase nickel hydroxide	95 °C, 1 w	1 : 1
ii	β_{SF}-$Ni(OH)_2$	Stacking faulted nickel hydroxide	50 °C, 2 d	1 : 1
iii	β_{IS}-$Ni(OH)_2$	Interstratified nickel hydroxide	5 °C, 1 w	1 : 1
iv	β-$Ni(OH)_2$	Beta-phase nickel hydroxide	95 °C, 1 w	1 : 2
v	β_{SF}-$Ni(OH)_2$	Stacking faulted nickel hydroxide	50 °C, 2 d	1 : 2
Vi	β_{IS}-$Ni(OH)_2$	Interstratified nickel hydroxide	5 °C, 1 w	1 : 2

formed at intermediate temperatures and ageing durations. Therefore, the conditions selected were based on the preliminary experiments summarised in Table S1† in order to ensure that the required material was reproducibly isolated. It was also found that changing the ratio of nickel(II) cations to hydroxide anions in solution so that the base would be in excess no longer had a significant effect on the disorder formation. At both a 1 : 3 and 1 : 4 ratio, only one type of disordered nickel hydroxide material was formed regardless of the temperature and ageing duration conditions used.

Six nickel hydroxide materials were targeted (Table 1) using three sets of temperature and ageing duration, each prepared using two potassium hydroxide solution concentrations to give a 1 : 1 and 1 : 2 ratio. Three distinct material types were identified through the powder X-ray diffraction analysis shown in Fig. 4a. The first material type formed at 95 °C over 1 week had narrow reflections that matched with the crystalline beta-phase of nickel hydroxide (β-$Ni(OH)_2$) as theophrastite (ICDD PDF 14-117).[18]

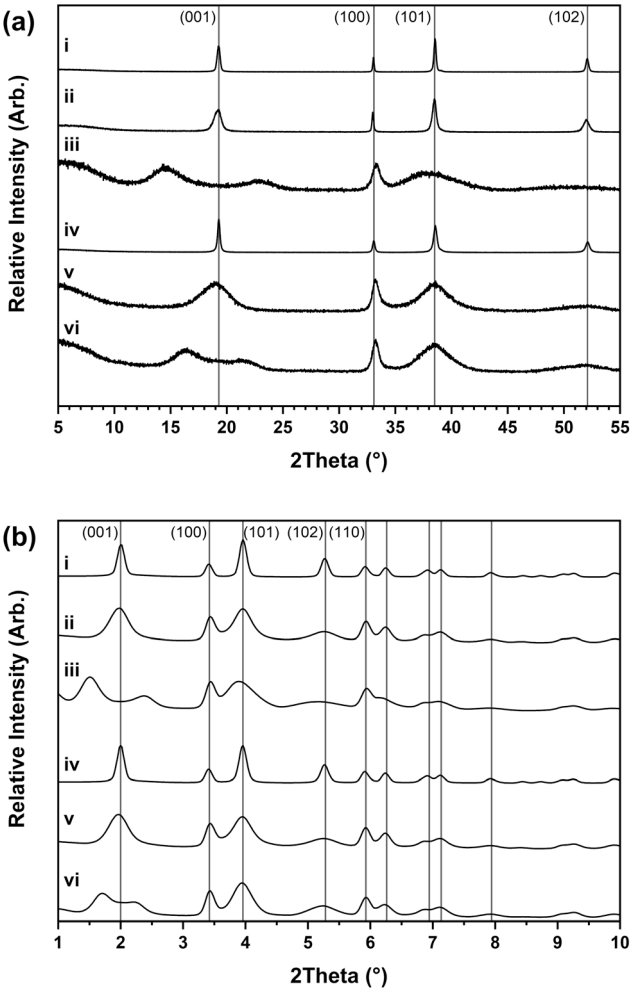

Fig. 4 Powder X-ray diffraction patterns collected with (a) Cu $K_{\alpha 1}$ (λ = 1.5406 Å) and (b) synchrotron (λ = 0.161669 Å) radiation of the i–vi nickel hydroxide materials. The *hkl* assignments given are of nickel hydroxide (ICDD PDF 14-117).

The second type that formed at 50 °C over 2 days had the same reflections as β-$Ni(OH)_2$ but with anisotropic peak widths where the 001, 101 and 201 are broader than the 100 which indicates beta-phase nickel hydroxide with stacking fault disorder (β_{SF}-$Ni(OH)_2$). The origin of this disorder is much more complex than might initially be expected from the description.[30,31] First Barnard[32] and then Tessier[33] described two structural dislocations which could lead to this unusual broadening of powder X-ray diffraction patterns. These dislocations are referred to as 'growth faults' and 'deformation faults' which typically occur because of rapid or low-temperature crystal growth. Broadening of the 00*l* reflections is commonly observed in the powder X-ray diffraction pattern of layered hydroxide materials since this group of reflections relates to disorder in the *c*-direction.[33–35] Additionally, *hk*0 broadening is also observed if the crystallites are small and there is good agreement between the size of the crystals with the broadening of both 00*l* and *hk*0 reflections, determined through the Debye–Scherrer formula and direct domain size determination by electron microscopy.[34] However, abnormal broadening can also be observed for the 10*l* and 20*l* (where *l* is not zero) which cannot be explained by particle size arguments alone.

The third material type formed at 5 °C over 1 week also had the broadened reflections of β-$Ni(OH)_2$ but with an apparent splitting of the 001 reflection, identified previously as characteristic of interstratification disorder (β_{IS}-$Ni(OH)_2$).[26,27] Structures with interstratified phases are described for clay minerals where there is a mix of two or more types of layers, *e.g.* dioctahedral and trioctahedral clays that are stacked in the *c*-direction of the unit cell, producing a wide range of mixed-layer clay phases, *e.g.* kaolinite-smectite and talc-smectite.[36,37] These interstratified phases produce powder X-ray diffraction patterns which are composites of the two types of layer, but often with much broadening in the observed reflections since long-range order in the *c*-direction is lost. Interstratification of the nickel hydroxides has been suggested to occur in the same way as clays, consisting of layers of both the beta-phase and the alpha-phase with interlayer species intermixed.[38,39] In contrast to other interstratified phases that are typically formed of two crystalline phases, the turbostratic alpha-phase of nickel hydroxide often has no long-range ordering to the structure. Therefore the diffraction patterns generated by interstratified nickel hydroxides are different to a simple mixture of the two independent crystalline phases and the reflections relating to the *c*-direction can be shifted, broadened or absent.[40] For example, in the powder X-ray diffraction patterns collected by Kamath[38,39] both the expected first reflection of the ordered alpha-phase (~7–10 Å) and beta-phase (~4.6 Å) are missing.

Fig. 4b shows high-resolution powder X-ray diffraction data collected for these materials using a synchrotron radiation source and the reflections observed for the β-$Ni(OH)_2$ and β_{SF}-$Ni(OH)_2$ materials match beta-phase nickel hydroxide but with differences in the crystallinity. The diffraction patterns of the β_{IS}-$Ni(OH)_2$ materials have broad and split 001 reflections with the maxima observed being different, with Fig. 4b(iii) having *d*-spacing values at ~6.12 Å and ~3.90 Å while in Fig. 4b(vi) at

~5.45 Å and ~4.16 Å. These values are also different from the interlayer *d*-spacing values expected in β-$Ni(OH)_2$ which is 4.60 Å and α-$Ni(OH)_2$ which is approximately between 7–10 Å.[11] This suggests these values are not derived from the interlayer distances of the parent phases similar to those usually observed in interstratified clay materials, implying the disorder in layered hydroxides is different. Since clays form in the earth over long periods through weathering, the layer arrangement can be more ordered with larger domains in the *c*-direction of a phase, making it possible to see reflections characteristic of the stacking sequences of the individual phases. In contrast, these nickel hydroxide formation experiments were carried out over short periods and crystals that formed rapidly are likely to be significantly smaller and have a less ordered structure.

Synchrotron X-ray pair distribution function (XPDF) analysis

The X-ray pair distribution function D(*r*) data in Fig. 5a were obtained from the collected synchrotron diffraction data to observe the local structure bonding environments present in the materials. The atomic pair distances observed are assigned in Table 2 to the expected atom pair distances extracted from the crystal structure of beta-phase nickel hydroxide (Fig. S1†). The intralayer values represent the distances between the atom pairs within a single nickel hydroxide layer formed by the metal-hydroxide octahedra. These distances are present in both the beta-phase and alpha-phases of nickel hydroxide and would be expected to be observed in all the materials. Interlayer distances will also be apparent due to the atom pairs across adjacent nickel hydroxide octahedral layers. These distances will only be present in the beta-phase but not the alpha-phase and changes or absences of these distances will indicate differences in the short-range layer stacking.

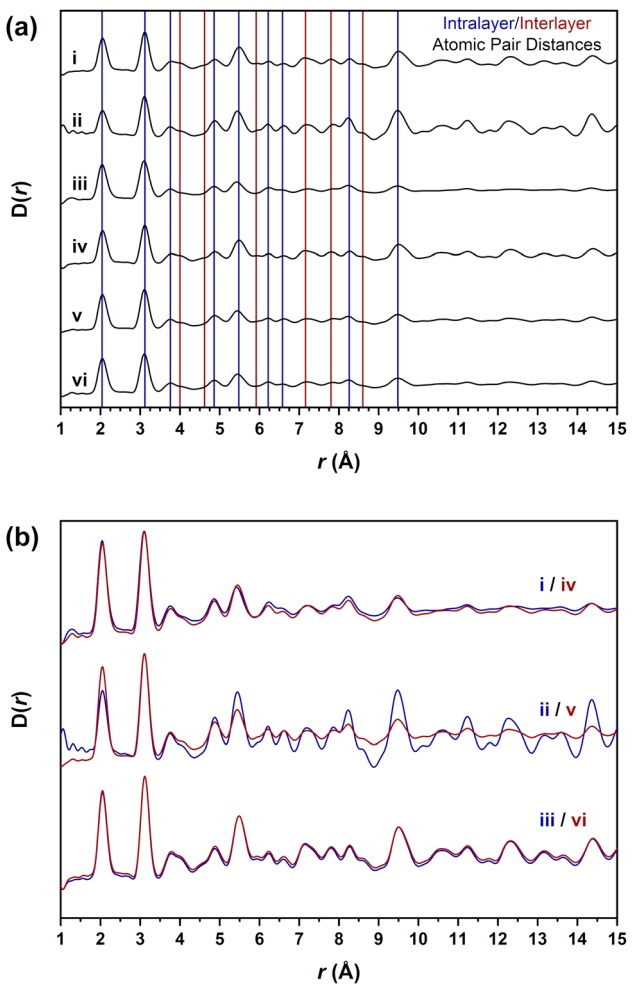

Fig. 5 X-ray pair distribution function data collected with synchrotron radiation (λ = 0.161669 Å) of the i–vi nickel hydroxide materials. (a) A comparison of the observed atomic pair distances to the interlayer and intralayer distances expected of beta-phase nickel hydroxide and (b) an overlay comparison of the individual material types.

Table 2 Atomic pair distances observed by X-ray pair distribution function analysis of the i–vi nickel hydroxide materials that are assigned to the intralayer and interlayer distances present in literature crystallographic data of β-$Ni(OH)_2$ as theophrastite[18]

Atomic pair assignment		XPDF atom pair distance (Å)					
Intralayer atom pair	**Distance (Å)**	**i**	**ii**	**iii**	**iv**	**v**	**vi**
Ni–O	2.13	2.04	2.06	2.06	2.06	2.06	2.06
Ni–Ni/O–O	3.11	3.12	3.10	3.10	3.12	3.10	3.10
Ni–O	3.77	3.76	3.76	3.76	3.76	3.76	3.76
Ni–O	4.88	4.86	4.88	4.86	4.88	4.88	4.86
Ni–Ni/O–O	5.39	5.48	5.44	5.42	5.50	5.44	5.44
Ni–Ni/O–O	6.22	6.22	6.24	6.24	6.24	6.22	6.22
O–O	6.88	6.58	6.62	6.58	6.62	6.62	6.62
Ni–Ni/O–O	8.24	8.26	8.26	8.24	8.26	8.26	8.26
Ni–Ni/O–O	9.34	9.48	9.46	9.48	9.50	9.48	9.50
Interlayer atom pair	**Distance (Å)**	**i**	**ii**	**iii**	**iv**	**v**	**vi**
Ni–O	3.90	4.00	4.06	—	4.04	4.06	—
Ni–Ni/O–O	4.62	4.62	—	—	4.60	—	—
Ni–O	5.88	5.92	5.96	—	5.92	—	—
O–O	7.15	7.16	7.18	7.22	7.14	7.18	7.20
Ni–Ni/O–O	7.75	7.80	7.80	7.84	7.82	7.84	7.82
O–O	8.40	8.60	8.58	—	8.62	8.62	—

The datasets in Fig. 5b are a direct overlay of the same β-$Ni(OH)_2$, β_{SF}-$Ni(OH)_2$ and β_{IS}-$Ni(OH)_2$ material types with both intralayer and interlayer distances in all of the materials assigned. These data show there is not a significant difference in the atomic pair distances present, with only the β_{SF}-$Ni(OH)_2$ materials having different relative peak intensities which are more intense in Fig. 5b(ii) and (v). While all of the intralayer distances up to 10 Å are accounted for across all materials, several interlayer distances present in the β-$Ni(OH)_2$ materials are absent in the disordered β_{SF}-$Ni(OH)_2$ and β_{IS}-$Ni(OH)_2$ examples. This suggests that the broadening observed in the diffraction data is due only to the long-range layer stacking disorder occurring along the *c*-direction of the unit cell. There is no change to the local short-range structure between these materials, indicating that regardless of the disorder, individual layers of octahedra are formed in all the materials studied. Therefore, it is not possible to establish any differences in the structures of these materials through these datasets and alternative methods are required.

Spectroscopic analysis of disordered nickel hydroxide materials

Spectroscopic analysis affords information on the bonding present in the different nickel hydroxide materials and importantly reveals the incorporation of nitrate anions from the nickel(II) salt reagent used in most of the samples analysed. Differences are observed in the infrared spectra in Fig. 6a and Raman spectra in Fig. 6b of the β-$Ni(OH)_2$, β_{SF}-$Ni(OH)_2$ and β_{IS}-$Ni(OH)_2$ material types. Crystalline β-$Ni(OH)_2$ materials have a highly ordered structure with no nitrate anions detected as observed in Fig. 6a(i) and b(i). The infrared spectrum in Fig. 6a(iv) shows no nitrate anions are detected but the Raman spectrum in Fig. 6b(iv) suggests a small amount to be present from a phase impurity. Differently, intense bands of nitrate are present in the disordered β_{SF}-$Ni(OH)_2$ and β_{IS}-$Ni(OH)_2$ types. The assignment of these bands listed in Table 3 allows for two nitrate anion symmetries to be identified which indicates there are different layered hydroxide structures present.

The nitrate in the β_{SF}-$Ni(OH)_2$ materials is present in a D_{3h} symmetry which has four vibrational modes that are A'_1, A''_2, and $2E'$ (ν_1 to ν_4) with ν_1 being infrared inactive and ν_2 being Raman inactive.[41–44] This anion symmetry is established in these materials by the infrared inactive nitrate symmetric stretch at ~1000 cm^{-1} which is absent in the infrared spectra but present in the Raman spectra. Moreover, the infrared spectra also have bands of water present including the broad O–H stretch at ~3500 cm^{-1} and the O–H bend at ~1650 cm^{-1}. Therefore, it can be predicted that the nitrate anions are hydrated with trigonal geometry and are incorporated between the layers similar to the anions present in layered double hydroxide structures. This suggests that the alpha-phase hydroxide is present and implies that materials described as β_{SF}-$Ni(OH)_2$ by powder diffraction are instead a mixture, or possibly an interstratification, between the beta-phase and alpha-phase nickel hydroxides.

The β_{SF}-$Ni(OH)_2$ types also have an intense Raman O–H stretch at ~3600 cm^{-1} in addition to the band at ~3580 cm^{-1} present in the β-$Ni(OH)_2$ materials. This has previously been identified as a unique feature of layer stacking faulted beta-phase nickel hydroxide.[45] The intensity of the band was shown to increase as the layer stacking in the *c*-direction became more disordered and was only observed to coexist with the parent beta-phase nickel hydroxide. In the case where both layered hydroxide phases are present, it can be expected that the differences in the crystallinity between the beta-phase and alpha-phase of nickel hydroxide would result in non-ideal layer stacking similar to what is described as simple layer disordering.

Nitrate anions in a D_{3h} symmetry are present in the β_{IS}-$Ni(OH)_2$ materials but there are also additional bands of the C_{2v} symmetry of nitrate observed. This nitrate symmetry is observed in layered metal hydroxynitrate structures where one N–O bond is in a different environment from the other two because the nitrate anions are covalently coordinated to the nickel(II)

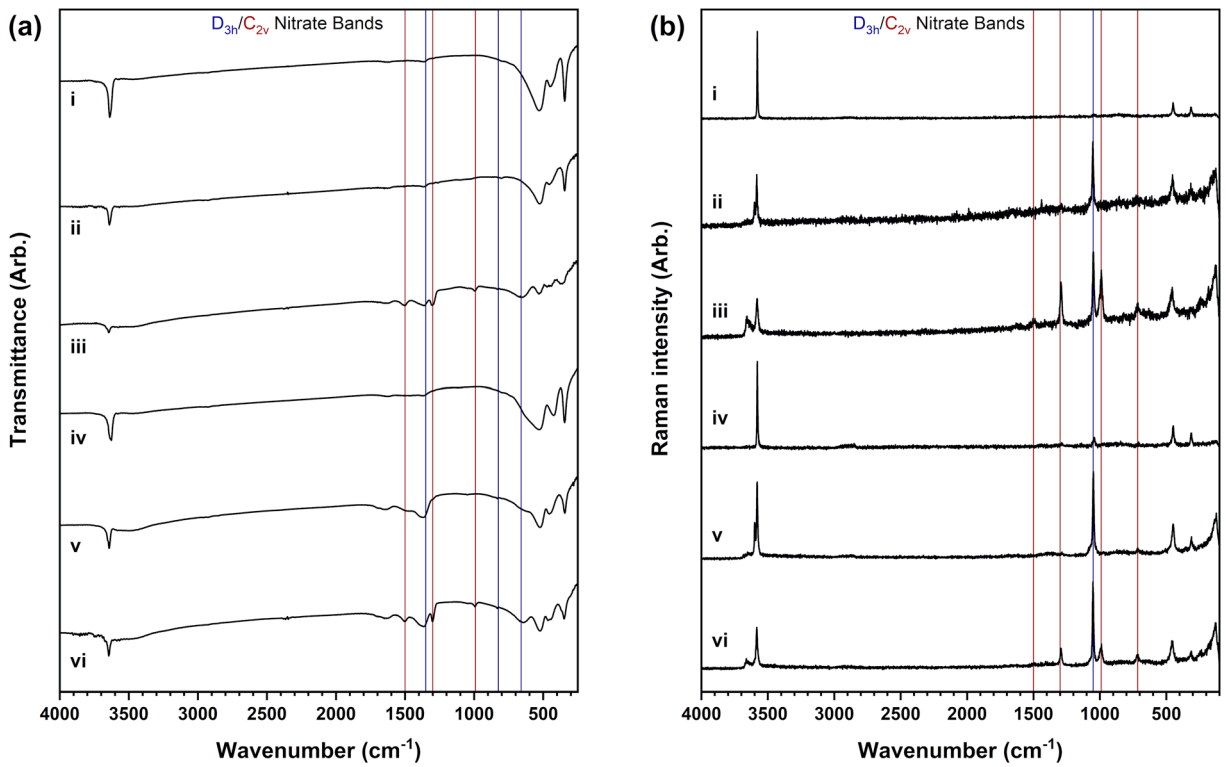

Fig. 6 (a) Infrared spectra and (b) Raman spectra of the i–vi nickel hydroxide materials. The vertical lines indicate nitrate bands, with the D_{3h} symmetry (blue lines) indicating loosely held nitrate between the layers in alpha-phase layered hydroxides as well as the cation coordinated C_{2v} symmetry (red lines) associated with layered hydroxynitrates.

Table 3 Assignment of the infrared and Raman bands present in the spectra collected of i–vi nickel hydroxide material types compared to literature spectroscopic data values[41–45]

Infrared band assignment		Ref. value	i	ii	iii	iv	v	vi
Hydroxide stretch	ν(O–H)	3570–3650	3638	3641	3647	3627	3643	3645
Hydroxide bend	δ(O–H)	510–553	542	531	532	532	529	533
Lattice modes	δ(Ni–O)	350–475	450	455	437	418	456	465
Hydroxide bend	γ(O–H)	340–354	345	345	348	345	344	349
Water stretch	ν(O–H)	∼3570–3650	—	—	∼3500	—	∼3500	∼3500
Water bend	δ(O–H)	1600–1650	—	—	1650	—	1647	1651
D_{3h} nitrate stretch (E′)	$\nu_{as}(NO_3)$	1350	—	1364	1378	—	1363	1368
D_{3h} nitrate bend (A''_2)	$\gamma(NO_3)$	830	—	831	838	—	834	833
C_{2v} nitrate stretch (B_2)	$\nu_s(NO_2)$	1400–1500	—	—	1514	—	—	1500
C_{2v} nitrate stretch (A_1)	ν_{as}(NO)	1290	—	—	1301	—	—	1303
C_{2v} nitrate stretch (A_1)	ν_s(NO)	1000	—	—	995	—	—	994
C_{2v} nitrate bend (B_2)	$\delta(NO_3)$	715	—	—	715	—	—	712
Raman band assignment		**Ref. value**	**i**	**ii**	**iii**	**iv**	**v**	**vi**
Hydroxide stretch	ν(O–H)	3580–3600	3580	3601, 3584	3659, 3580	3580	3600, 3580	3662, 3583
Hydroxide bend	γ(O–H)	306–319	315	315	315	314	311	313
Lattice modes	δ(Ni–O)	445–450	450	453	455	449	448	455
D_{3h} nitrate stretch (A'_1)	$\nu_s(NO_3)$	1050	—	1052	1050	1047	1049	1052
C_{2v} nitrate stretch (B_2)	$\nu_s(NO_2)$	1400–1500	—	—	1498	—	—	1503
C_{2v} nitrate stretch (A_1)	ν_{as}(NO)	1290	—	—	1294	—	—	1293
C_{2v} nitrate stretch (A_1)	ν_s(NO)	1000	—	—	988	—	—	989
C_{2v} nitrate bend (B_2)	$\delta(NO_3)$	715	—	—	714	—	—	718

cations through the oxygen atoms (Fig. S2†).[42] This behaviour can be identified through the six vibrational modes of the C_{2v} symmetry that arise due to the splitting of the two doubly degenerate (E′) modes of D_{3h} symmetry and are all infrared and Raman active.[41–44] Not all six bands expected for C_{2v} nitrate are observed, however, the symmetric N–O stretch that is infrared inactive for the D_{3h} symmetry is observed in both the infrared and Raman spectra at ∼1000 cm^{-1}. The change in the infrared activity of this band between the alpha-phase hydroxide and hydroxynitrate phases allows for a diagnostic method of determining if hydroxynitrate phases are present in mixed-phase materials.

The position of the symmetric N–O stretching band can also be used to identify the nickel hydroxynitrate phase present by comparison to spectroscopic data collected on the individual nickel hydroxynitrate phases (Fig. S3†). Three nickel hydroxynitrate phases were targeted by different synthesis methods, namely $Ni_2(OH)_3(NO_3)$ (where $x = 0.5$) by Petrov precipitation,[46] $Ni_3(OH)_4(NO_3)_2$ (where $x = 0.67$) by nickel(II) nitrate thermolysis[28] and $Ni(OH)(NO_3)\cdot H_2O$ (where $x = 1.0$) by mechanochemical methods.[47] The band positions in Fig. 6b(iii) and (vi) correlate to those of $Ni_3(OH)_4(NO_3)_2$ (where $x = 0.67$) that are observed at 984 cm^{-1} in the infrared and 974 cm^{-1} in the Raman data. This was the phase determined because the values of $Ni(OH)(NO_3)\cdot H_2O$ (where $x = 1.0$) are higher at ∼1050 cm^{-1} while $Ni_2(OH)_3(NO_3)$ (where $x = 0.5$) could not be prepared and instead a mixed-phase product was formed. The presence of nitrate in a C_{2v} symmetry determined in the β_{IS}-$Ni(OH)_2$ materials suggests phase interstratification disorder is not a simple mixture or an interstratification between only the beta-phase and alpha-phase hydroxides as previously reported by Kamath[39] because there are multiple disordered phases present. While the nitrate in C_{2v} symmetry could be observed due to any remaining nickel(II) nitrate starting reagent, it is not detected as an impurity phase by powder diffraction analysis. The Raman band position of the nitrate symmetric N–O stretch is also observed to be higher in the nickel(II) nitrate reagent at 1057 cm^{-1} (Fig. S4†) than any of the layered hydroxide phases. In addition, if the interstratification was solely between alpha-phase and beta-phase nickel hydroxides, the nitrate would only be present as loosely coordinated anions between the layers with D_{3h} symmetry and the covalently bonded nitrate anions in C_{2v} symmetry would not be observed. This suggests that the materials described with interstratification disorder can be considered an extension of the β_{SF}-$Ni(OH)_2$ materials that have both the alpha-phase and beta-phase hydroxides, but with the nickel hydroxynitrate phase $Ni_3(OH)_4(NO_3)$ additionally present.

These findings suggest that the previous concepts of stacking faulted and interstratified disorder in nickel hydroxide

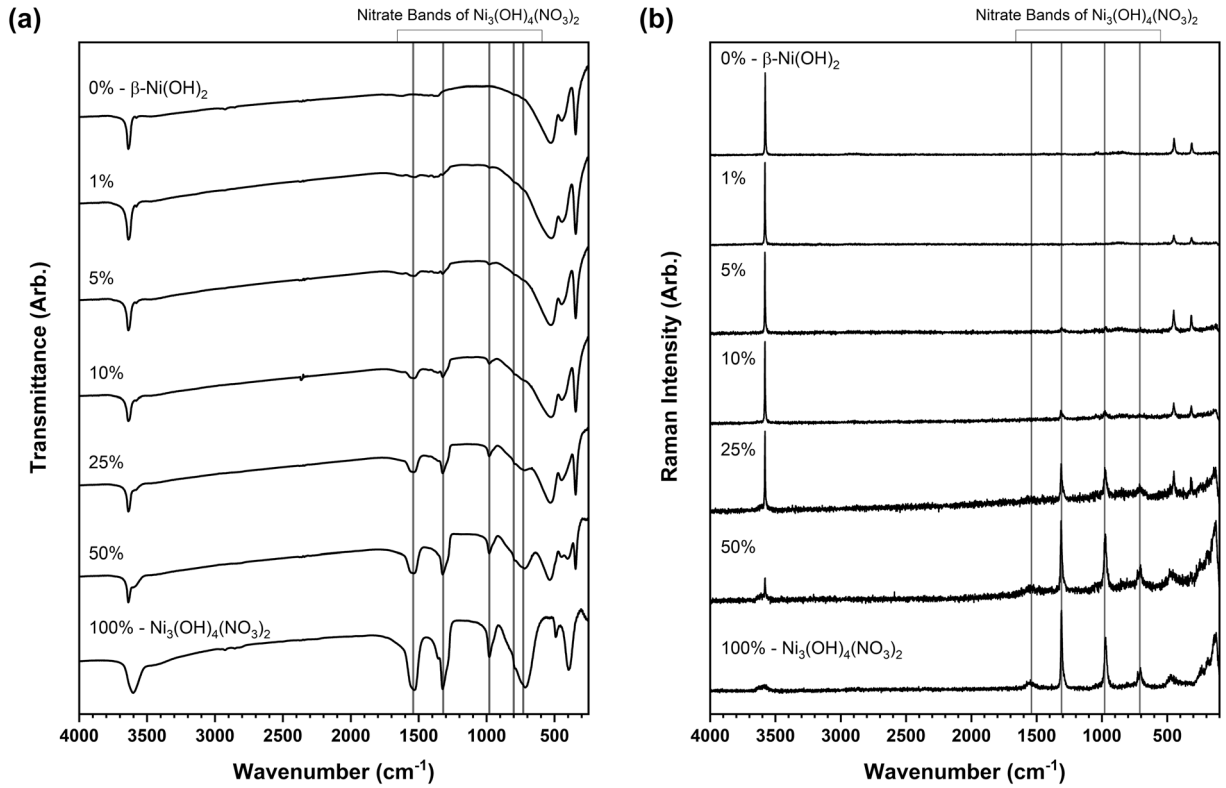

Fig. 7 (a) Infrared absorption spectra as CsI disks and (b) Raman spectra collected for the standard mixtures formed between β-$Ni(OH)_2$ and the layered hydroxynitrate $Ni_3(OH)_4(NO_3)_2$ at 0, 1, 5, 10, 25, 50 and 100 wt% intervals.

materials are more complex than the simple structural disorder concepts they are named after. The broadening of the beta-phase nickel hydroxide reflections typically attributed to stacking faults is instead likely a result of an interstratification of the beta-phase and alpha-phases hydroxides. Similarly, materials with split beta-phase nickel hydroxide 001 reflections attributed to the phase interstratified disorder are also instead multi-phase with both beta-phase and alpha-phase nickel hydroxides as well as nickel hydroxynitrate phases present. It is proposed that these are more plausible as interstratification of multiple phases with the beta-phase and alpha-phase hydroxides intergrown. This is in contrast to a simple mixture of the phases which would have reflections corresponding to the individual phases that would indicate regions of ordered layering in the *c*-direction of the unit cell.

Nickel hydroxynitrate identification in mixed-phase materials

The ability to identify impurity phases is crucial from a practical application standpoint for developing phase-pure materials with predictable electroactive properties. The detection of layered hydroxynitrate phases in these materials is exceedingly difficult by powder X-ray diffraction analysis which is unsuitable as the sole characterisation method for these materials. Features in the infrared and Raman spectroscopy datasets, particularly the different bonding and vibrational band positions of the nitrate anions, offer conclusive identities of the layered hydroxide and hydroxynitrate phases present. However, this ability is limited only to a few polyatomic anions that display the differences in symmetry required such as nitrates and carbonates. This makes it difficult to identify phases where for example nickel(II) halide starting reagents are used. To examine whether small amounts of a nickel hydroxynitrate

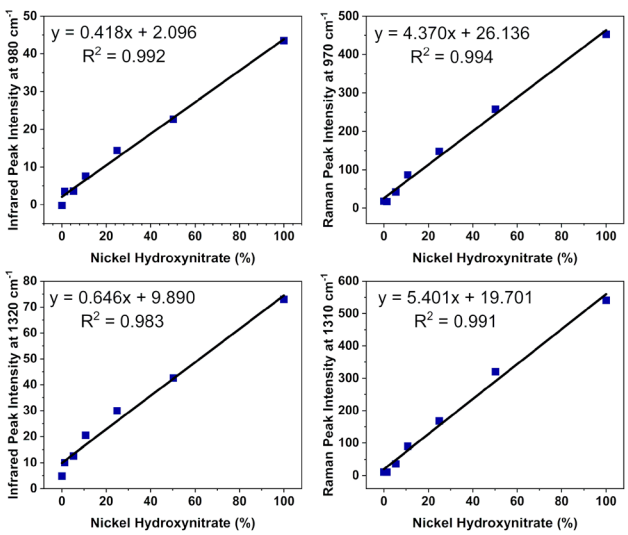

Fig. 8 Calibration plots showing the linear relationship between the background-corrected intensity observed of the C_{2v} nitrate infrared band at 980 cm^{-1} and 1320 cm^{-1} as well as Raman band at 970 cm^{-1} 1310 cm^{-1} with the weight percentage (wt%) proportion of nickel hydroxynitrate present.

Table 4 Determined amounts of nickel hydroxynitrate present in the i–vi nickel hydroxide materials

Nickel hydroxide material	Assignment by powder X-ray diffraction	Phase(s) identified by infrared and Raman spectroscopy	Wt% of nickel hydroxynitrate (infrared data)	Wt% of nickel hydroxynitrate (Raman data)	TGA weight loss (%)	Additional TGA weight loss from β-$Ni(OH)_2$
i	β-$Ni(OH)_2$	β-$Ni(OH)_2$	0.6 (±6.1)	<0.1 (±1.5)	20.2	+0.8
ii	β_{SF}-$Ni(OH)_2$	β-$Ni(OH)_2$ and α-$Ni(OH)_2$	5.0 (±6.4)	0.9 (±0.5)	21.6	+2.2
iii	β_{IS}-$Ni(OH)_2$	β-$Ni(OH)_2$, α-$Ni(OH)_2$, and $Ni_3(OH)_4(NO_3)_2$	33.1 (±32.4)	58.4 (±26.1)	31.7	+12.3
iv	β-$Ni(OH)_2$	β-$Ni(OH)_2$	6.3 (±2.0)	<0.1 (±3.7)	20.3	+0.9
v	β_{SF}-$Ni(OH)_2$	β-$Ni(OH)_2$ and α-$Ni(OH)_2$	11.4 (±19.4)	2.4 (±0.5)	26.5	+7.1
vi	β_{IS}-$Ni(OH)_2$	β-$Ni(OH)_2$, α-$Ni(OH)_2$, and $Ni_3(OH)_4(NO_3)_2$	35.0 (±36.6)	37.1 (±15.3)	29.2	+9.8

phase could be detected and quantified by spectroscopic analysis in disordered materials, standard mixtures were prepared of β-$Ni(OH)_2$ and $Ni_3(OH)_4(NO_3)_2$ at different proportions. These phases were selected as they were identified in the disordered materials and were used to form mixtures at five intervals between 1 and 50 wt% with the two pure phases forming 0 and 100 wt%. Powder X-ray diffraction data were also collected on these standard mixture samples (Fig. S5†) and the intensities of the individual phase reflections were found to also increase as the wt% increased. However, as the diffraction patterns of the disordered phases do not have the specific reflections of the phases identified (Fig. 4), a similar analysis approach could not be performed.

Fig. 7a and b show the infrared and Raman spectra respectively of the standard mixture samples prepared where the band intensity of the C_{2v} symmetry nitrate increased with increased wt%. Calibration plots were prepared from the datasets using the intensities of the infrared and Raman band which were background corrected using an average intensity between 1150–1200 cm^{-1}, a region where there are no vibrational modes expected for the hydroxide or hydroxynitrate phases. Fig. 8 shows regression analysis gave a good fit of the calibration plots, indicating linear correlations between the amount of C_{2v} nitrate present and the peak intensities of the infrared bands at 980 and 1320 cm^{-1} as well as the Raman bands at 970 cm^{-1} and 1310 cm^{-1}. These plots were used to estimate the amount of $Ni_3(OH)_4(NO_3)_2$ present in the i–vi nickel hydroxide materials and the results are listed in Table 4.

Through this analysis, it was determined that the β-$Ni(OH)_2$ and β_{SF}-$Ni(OH)_2$ type materials contained small quantities of the layered hydroxynitrate phase, varying somewhat by technique at ~10 wt% by infrared but only ~5 wt% by Raman. In contrast, considerable amounts of layered hydroxynitrate were present in the β_{IS}-$Ni(OH)_2$ type materials, determined to be in the approximate ranges of 30 to 35 wt% by infrared and 35 to 60 wt% by Raman. The variation between the values obtained by infrared and Raman as well as the observed errors on each value result from several sources, including inhomogeneity of the samples, variations in instrument resolution and band width, and significant differences in background intensity leading to more difficult background subtraction. Comparing the two, the Raman datasets have lower backgrounds and more narrow bands and these data are likely to be more reliable. There is also a difference in the samples analysed, where the standard mixtures were physical mixtures of crystallites of the individual phases whereas the disordered materials are proposed to be an interstratification of the nickel hydroxide phases. Despite this, however, the analysis shows that the interstratified phases have significant amounts of the impurity hydroxynitrate present.

The phases identified in the six nickel hydroxide materials are supported by the total weight losses listed in Table 4 determined by TG analysis and additional weight losses in the profile (Fig. S6†). The difference in the values obtained to the 19.4% theoretical weight loss of beta-phase nickel hydroxide are also listed and are within 1% for the β-$Ni(OH)_2$ type materials. The weight loss values are slightly higher for the β_{SF}-$Ni(OH)_2$ materials which would be expected from the hydrated nitrate anions present in alpha-phase nickel hydroxide (Fig. S7†). If these materials were solely only stacking faulted beta-phase nickel hydroxide, the weight loss value should match the expected value for β-$Ni(OH)_2$. The β_{IS}-$Ni(OH)_2$ type materials have significantly higher weight losses than the β-$Ni(OH)_2$ and β_{SF}-$Ni(OH)_2$ types, being approximately at the midpoint between the values of β-$Ni(OH)_2$ at 19.4% and $Ni_3(OH)_4(NO_3)_2$ at 39.1%. Furthermore, there is a weight loss visible between 250 and 400 °C that is characteristic of the $Ni_3(OH)_4(NO_3)_2$ phase (Fig. S7†) as well as the low temperature loss indicative of coordinated water in the alpha phase. This is consistent with the wt% of the hydroxynitrate phases determined by Raman spectroscopy, but because there are three phases identified and significant overlap between alpha phase and hydroxynitrate phase weight losses, quantification of the individual phases is not possible.

This analysis further highlights the complexity of studying poorly crystalline nickel hydroxides and emphasises that assigning layered hydroxide phases based on the diffraction patterns alone is not sufficient. Spectroscopic techniques together with thermogravimetric analysis can be used, not only to identify the different phases in the poorly crystalline and disordered nickel hydroxide materials but to approximate their relative proportions. This was possible due to nitrate anions being present from the nickel(II) nitrate starting reagents used during synthesis that were incorporated with different symmetries into the layered structures. The approach described here

would be universally applicable to all layered metal hydroxide materials, including layered hydroxysalts and layered double hydroxide where polyatomic anions are present.[48–50]

Conclusions

Beta-phase nickel hydroxide materials with stacking fault and phase interstratification disorder can be targeted through the careful control of time and temperature during chemical precipitation synthesis. X-ray diffraction techniques including synchrotron X-ray pair distribution function analyses were unable to distinguish between different materials, and instead, only indicated long-range disorder with no change to the short-range intralayer and interlayer atomic pair distances. Characterisation using infrared and Raman spectroscopy identified different nitrate anion geometries present in the disordered materials, with the D_{3h} symmetry species present in the stacking faulted materials and both D_{3h} and C_{2v} symmetries present in the phase interstratified materials. This indicates the materials considered to be disordered are multi-phase materials with the indication that alpha-phase nickel hydroxide and nickel hydroxynitrate phases are formed. The amount of nickel hydroxynitrate in the interstratified β_{IS}-$Ni(OH)_2$ materials was also estimated using standard mixtures prepared between β-$Ni(OH)_2$ and $Ni_3(OH)_4(NO_3)_2$, being present at approximately 30 to 60 wt%. This was not detectable by powder X-ray diffraction methods meaning it is insufficient to characterise layered hydroxide materials by these methods alone.

Author contributions

Kurt Lawson: methodology, investigation and writing – original draft. Sam Wallbridge: methodology, investigation and writing – original draft. Amy Catling: methodology and investigation. Caroline Kirk: review and editing, supervision, project administration and funding acquisition Sandra Dann: conceptualization, resources, writing – original draft, review and editing, supervision, project administration and funding acquisition.

Conflicts of interest

There are no conflicts to declare.

Acknowledgements

We thank the ESPRC/STFC for funding for KL and the University for the DTP/EPSRC for the Studentship for SW. SCI are also thanked for their award of the Sydney Andrew Scholarship for SW.

References

1 J. McBreen, *Handbook of Battery Materials*, VCH, 1997.
2 H. Cheng, A. D. Su, S. Li, S. T. Nguyen, L. Lu, C. Y. H. Lim and H. M. Duong, *Chem. Phys. Lett.*, 2014, **601**, 168–173.
3 M. Aghazadeh, M. Ghaemi, B. Sabour and S. Dalvand, *J. Solid State Electrochem.*, 2014, **18**, 1569–1584.
4 T. Brezesinski, J. Wang, S. H. Tolbert and B. Dunn, *Nat. Mater.*, 2010, **9**, 146–151.
5 X. Yi, H. Sun, N. Robertson and C. Kirk, *Sustainable Energy Fuels*, 2021, **5**, 5236–5246.
6 R. J. Mortimer, M. Z. Sialvi, T. S. Varley and G. D. Wilcox, *J. Solid State Electrochem.*, 2014, **18**, 3359–3367.
7 Y. Chen, K. Rui, J. Zhu, S. X. Dou and W. Sun, *Chem.–Eur. J.*, 2019, **25**, 703–713.
8 H. Bode, K. Dehmelt and J. Witte, *Electrochim. Acta*, 1966, **11**, 1079–1087.
9 D. S. Hall, D. J. Lockwood, C. Bock and B. R. MacDougall, *Proc. R. Soc. A*, 2015, **471**, 20140792.
10 T. Marcopoulos and M. Economou, *Am. Mineral.*, 1981, **66**, 1020–1021.
11 R. S. McEwen, *J. Phys. Chem.*, 1971, **75**, 1782–1789.
12 A. Szytula, A. Murasik and M. Balanda, *Phys. Status Solidi*, 1971, **43**, 125–128.
13 C. Greaves and M. A. Thomas, *Acta Crystallogr., Sect. B: Struct. Crystallogr. Cryst. Chem.*, 1986, **42**, 51–55.
14 M. Mookherjee and L. Stixrude, *Am. Mineral.*, 2006, **91**, 127–134.
15 P. Oliva, J. Leonardi, J. F. Laurent, C. Delmas, J. J. Braconnier, M. Figlarz, F. Fievet and A. d. Guibert, *J. Power Sources*, 1982, **8**, 229–255.
16 A. Livingstone and D. L. Bish, *Mineral. Mag.*, 1982, **46**, 1–5.
17 C. Faure, C. Delmas and M. Fouassier, *J. Power Sources*, 1991, **35**, 279–290.
18 R. W. Cairns and E. Ott, *J. Am. Chem. Soc.*, 1933, **55**, 527–533.
19 O. Glemser and J. Einerhand, *Z. Anorg. Chem*, 1950, **261**, 43–51.
20 P. V. Kamath, G. H. Annal Therese and J. Gopalakrishnan, *J. Solid State Chem.*, 1997, **128**, 38–41.
21 K. Petrov, N. Zotov, E. Mirtcheva, O. García-Martínez and R. M. Rojas, *J. Mater. Chem.*, 1994, **4**, 611–614.
22 P. Gallezot and M. Prettre, *Bull. Soc. Chim.*, 1969, **2**, 407–409.
23 M. Louër, D. Louër and D. Grandjean, *Acta Crystallogr., Sect. B: Struct. Crystallogr. Cryst. Chem.*, 1973, **29**, 1696–1703.
24 B. Bovio and S. Locchi, *J. Crystallogr. Spectrosc. Res.*, 1982, **12**, 507–517.
25 M. Louër, D. Grandjean and D. Weigel, *Acta Crystallogr., Sect. B: Struct. Crystallogr. Cryst. Chem.*, 1973, **29**, 1703–1706.
26 L. Eriksson, D. Louër and P.-E. Werner, *J. Solid State Chem.*, 1989, **81**, 9–20.
27 M. Bianchini, M. Roca-Ayats, P. Hartmann, T. Brezesinski and J. Janek, *Angew. Chem., Int. Ed.*, 2019, **58**, 10434–10458.
28 T. Biswick, W. Jones, A. Pacuła and E. Serwicka, *J. Solid State Chem.*, 2006, **179**, 49–55.
29 N. Iyi, F. Geng and T. Sasaki, *Chem. Lett.*, 2009, **38**, 808–809.
30 D. F. Wong, K. Young, L. Wang, J. Nei and K. Y. S. Ng, *J. Alloys Compd.*, 2017, **695**, 1763–1769.
31 T. N. Ramesh, *Mater. Chem. Phys.*, 2009, **114**, 618–623.
32 R. Barnard, C. F. Randell and L. F. Tye, *Power Sources*, 1980, **8**, 401–425.
33 C. Delmas and C. Tessier, *J. Mater. Chem.*, 1997, **7**, 1439–1443.
34 C. Tessier, *J. Electrochem. Soc.*, 1999, **146**, 2059–2067.

35 T. N. Ramesh and P. V. Kamath, *Mater. Res. Bull.*, 2008, **43**, 2827–2832.
36 R. C. Reynolds, *Crystal Structures of Clay Minerals and Their X-Ray Identification*, Mineralogical Society of Great Britain and Ireland, 1980.
37 J. Cuadros, *Clay Miner.*, 2012, **47**, 147–164.
38 M. Rajamathi, P. Vishnu Kamath and R. Seshadri, *J. Mater. Chem.*, 2000, **10**, 503–506.
39 M. Rajamathi, G. N. Subbanna and P. Vishnu Kamath, *J. Mater. Chem.*, 1997, **7**, 2293–2296.
40 L. Guerlou-Demourgues, C. Denage and C. Delmas, *J. Power Sources*, 1994, **52**, 269–274.
41 K. Nakamoto, *Handbook of Vibrational Spectroscopy*, Wiley, 2006.
42 D. N. Sathyanarayana, *Vibrational Spectroscopy: Theory and Applications*, New Age International Limited, 2015.
43 G. Adachi, N. Imanaka and Z. C. Kang, *Binary Rare Earth Oxides*, Springer, Netherlands, 2006.
44 V. R. Sastri, J. R. Perumareddi, V. R. Rao, G. V. S. Rayudu and J. C. G. Bünzli, *Modern Aspects of Rare Earths and Their Complexes*, Elsevier Science, 2003.
45 D. S. Hall, D. J. Lockwood, S. Poirier, C. Bock and B. R. MacDougall, *J. Phys. Chem. A*, 2012, **116**, 6771–6784.
46 L. Markov, K. Petrov and V. Petkov, *Thermochim. Acta*, 1986, **106**, 283–292.
47 N. Thomas, *Mater. Res. Bull.*, 2012, **47**, 3568–3572.
48 Z. Pan, Y. Jiang, P. Yang, Z. Wu, W. Tian, L. Liu, Y. Song, Q. Gu, D. Sun and L. Hu, *ACS Nano*, 2018, **12**, 2968–2979.
49 X. Liu, R. Ma, Y. Bando and T. Sasaki, *Adv. Mater.*, 2012, **24**, 2148–2153.
50 Y. Jiang, Y. Song, Y. Li, W. Tian, Z. Pan, P. Yang, Y. Li, Q. Gu and L. Hu, *ACS Appl. Mater. Interfaces*, 2017, **9**, 37645–37654.